A Recoverable Strain-Based Model for Flow-Induced Crystallization

*Gerrit W. M. Peters**, *Frank H.M. Swartjes, Han E. H. Meijer*

Materials Technology Group (www.mate.tue.nl), Dutch Polymer Institute, Eindhoven University of Technology, P.O. Box 513, 5600 Mb Eindhoven, The Netherlands

Summary: A model for the combined processes of quiescent and flow-induced crystallization of polymers is presented. This modeling should provide the necessary input data, in terms of the structure distribution in a product, for the prediction of mechanical properties and shape- and dimensional-stability. The model is partly based on the work of Schneider et al. [1] and Eder et al. [2] where the shear rate was taken as the relevant parameter for flow-induced crystallization. Rather then the shear rate as the driving force, a viscoelastic approach is proposed here, where the resulting recoverable strain (expressed by the elastic Finger tensor) with the highest relaxation time is the driving force for flow-induced crystallization. Thus we focus on the polymer that experiences the flow, rather then on the flow itself. For a fully characterized isotactic Polypropylene (iPP), i.e. a polymer for which all data needed as input for the computational model are available, comparison with experimental results from literature shows good agreement. For results from extensional flow, part of this data set is missing and therefore comparison is only qualitative.

Introduction

A new model for the combined processes of quiescent and flow-induced crystallization of polymers is presented. The final goal of this work is to predict, in detail, the spatial distribution of the crystalline structure in a product and, from that, the final mechanical properties and the shape- and dimensional-stability of the product. This paper is restricted to the modeling of the processing part. In a related paper in this special issue, Schrauwen et al. [3], the focus is on the relation between structure and mechanical properties. The present model for flow-induced nucleation and crystallization is based on a combination of experiments from literature (Eder et al. [2],Vleeshouwers and Meijer [4], Jerschow [5]) and a full description of the thermo-mechanical history of these experiments.

Crystallization of polymers is kinetically controlled and the motion involved refers to the transport of molecules from the disordered liquid phase to the ordered solid phase. The crystallization process can be subdivided into three stages. (a) Nucleation, which for a quiescent melt can be described by a Poisson point process. In case of flow,

 CCC 1022-1360/00/$ 17.50+.50/0

nuclei can be created by flow-induced ordering phenomena in the melt. (b) Growth. The nuclei formed will grow depending on the thermo-mechanical history they experienced. If the nuclei are sufficiently strained, they will grow into threads (shish), otherwise the stay spherical and will grow further radially (into spherulites). In both cases lamellar growth takes place that results in a shish-kebab structure for the thread-like nuclei. In the spherulites the lamella are present like spokes in a wheel. (c) Perfectionating. That is the process of improvement of the interior crystalline structure of the crystalline regions. This is also referred to as secondary crystallization.

Crystallization of polymers is influenced by the thermo-mechanical history during processing. Dependent on the amount of strain, experienced during flow, and the corresponding thermal history, the number, and type, of formed nuclei will be different as will the final crystalline structure. For example, the absence of shear in the center of an injection molded product results in a spherulitical structure, while in the highly strained regions near the cavity walls a shish-kebab structure can be present (Figure 1). It is this internal structure that determines the final product properties.

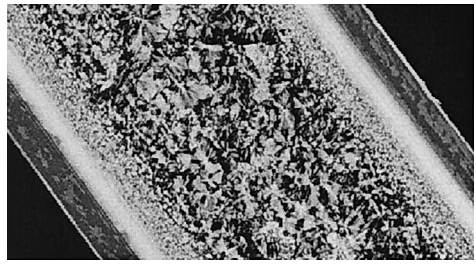

Figure 1. Cross section of an injection molded product.

In this paper we present a model for combined quiescent and Flow Induced Crystallization (FIC). The latter is based on the local molecular orientation as derived from an appropriate viscoelastic model of the polymer during flow. Two sets of differential equations, for quiescent and flow induced crystallization, respectively, give a full description of the growth of the internal structure depending on the local thermo-mechanical history of the polymer. Structure and rheological behavior are coupled. Based on results of Vleeshouwers and Meijer [5], who detected a pronounced influence of molar mass on shear induced crystallization, it is postulated that thread-like growth is governed by the high-end tail of the molecular mass distribution, which is characterized

by its largest relaxation time. This relaxation time is, on the other hand, a function of the nucleation density. Computational results are compared with experiments to demonstrate the model features.

Modeling

Viscoelastic stresses in a polymer melt are a result from the molecular orientation and stretch. If the viscoelastic stress (or a related measure, such as recoverable strain) is used as a fingerprint of the molecular state driving the flow induced nucleation and growth, the model for these stresses should be, consequently, quantitative. For shear dominated flows, as is the case in injection molding, a multi-mode Leonov model can be successfully applied. This model has the advantage that in first instance for its full description only linear viscoelastic data are needed. In case of more complex, combined shear and extensional flows more realistic quantitative viscoelastic models like the Pompom model are required, see for example Verbeeten et al. [6] and Swartjes [7]. Consequently, before presenting any models for (quiescent and) flow induced crystallization, viscoelastic models should be, necessarily, given some attention.

Viscoelastic Constitutive models

The Cauchy stress tensor σ is related to the recoverable strain tensor $\mathbf{B}_e$ by

$$\sigma = G_0 \mathbf{B}_e \tag{1}$$

in which G_0 the elastic modulus. The extra stress τ is defined by

$$\tau = G_0 (\mathbf{B}_e - \mathbf{I}) \tag{2}$$

For a realistic description of melt behavior a multi-mode mode should be applied

$$\boldsymbol{\sigma} = -\mathrm{p}\mathbf{I} + \sum_{\mathrm{i}}^{\mathrm{n}} \boldsymbol{\tau}_i \tag{3}$$

in which p the hydrostatic pressure. Once the viscoelastic stress is known, the recoverable strain is also defined, using Eq. 1. (Notice that for a multi-mode model also multiple recoverable strains are defined which do not represent the macroscopic

recoverable strain observed after unloading a sample. Every mode represents the recoverable strain of the molecules that have the corresponding relaxation time and it is imagined that this strain would be observable when unloading in absence of all other classes of molecules represented by different relaxation times). Here, we will distinguish between the viscoelastic models in terms of their stress, since this is common use.

Leonov model

The Leonov model is, like the upper convected Maxwell model (UCM), completely determined by linear viscoelastic data only, i.e. the set of moduli and relaxation times that can be easily obtained from small amplitude oscillatory shear flow. It describes the non-linear viscoelastic behavior of a polymeric liquid in shear rather well, provided that multi modes are used. Elongation behavior is, however, only poorly covered, Larson [8]. The differential equation reads:

$$\overset{\nabla}{\tau} + \frac{1}{\lambda}\tau + \frac{1}{2G_0\lambda}\tau\cdot\tau - \frac{1}{6G_0\lambda}[I_{(\tau+G_0 I)} - G_0^2 I_{(\tau+G_0 I)^{-1}}](\tau + G_0\mathbf{I}) = 2G_0\mathbf{D} \qquad (4)$$

in which I_A is the first invariant (the trace) of tensor A.

Extended Pompom model

The Pompom model, see McLeish and Larson [9] is based on an idealized molecule, the 'Pompom', which consists of a backbone with an equal number of branches at each end. A key feature in this model is the separation of stretch and orientation of a polymer molecule. Verbeeten et al. [6] proposed an extended version of the model (XPP), which predicts a second normal, stress difference and, moreover, gives a completely smooth behavior in extensional flows. Excellent quantitative agreement with measurements of branched (LDPE) and linear polymers (HDPE) was found, by using a multi mode version, in complex (shear combined with elongation) flows, Verbeeten et al. [6]. Even for a much more limited data set, Swartjes [7] also obtained a good fit of his viscometric data of the different iPP's with the XPP model as used in this paper. In the Pompom model, ensembles of equivalent Pompom molecules represent the different modes. The differential equation of the extended Pompom model (XPP) is given by

$$\overset{\nabla}{\tau} + \lambda(\tau)^{-1}.\tau = 2G_0\mathbf{D} \qquad (5)$$

with relaxation tensor

$$\lambda(\tau)^{-1} = \frac{1}{\lambda_{0b}}\left[\frac{\alpha}{G_0}\tau + \frac{1}{f(\tau)}\mathbf{I} + \underbrace{G_0\left(\frac{1}{f(\tau)} - 1\right)}_{a}\tau^{-1}\right] \tag{6}$$

while

$$\frac{1}{\lambda_{0b} f(\tau)} = \underbrace{\frac{2}{\lambda_s}\left(1 - \frac{1}{\Lambda}\right)}_{b} + \underbrace{\frac{1}{\lambda_{0b}\Lambda^2}\left(1 - \frac{aI_{\tau:\tau}}{3G_0^2}\right)}_{c} \tag{7}$$

The relaxation time λ_{0b} represents the orientation relaxation of the backbone, following from the orientation tensor $\boldsymbol{S}$, which is defined by:

$$\boldsymbol{S} = \frac{\sigma}{tr(\sigma)} = \frac{\mathbf{B}_e}{tr(\mathbf{B}_e)} \tag{8}$$

The backbone stretch (related to $I_{\mathbf{B}_e} = tr(\mathbf{B}_e)$) and the stretch relaxation time are defined as, respectively,

$$\Lambda = \sqrt{1 + \frac{I_\tau}{3G_0}} = \sqrt{\frac{I_{\mathbf{B}_e}}{3}} \tag{9}$$

$$\lambda_s = \lambda_{os}\exp(-\nu(\Lambda - 1)) \tag{10}$$

$$\nu = \frac{2}{q} \tag{11}$$

in which q is the number of branches. The parameter $a\,(a \geq 0)$ describes a Giesekus type of anisotropy, see Bird et al. [10]. This parameter influences the second normal stress difference only. The Extended Pompom model is equivalent to the original approximative Pompom model once $a = 0$. The orientation relaxation times of the backbone λ_{ob} are obtained from linear viscoelastic data. The number of branches q, the stretch relaxation times λ_s and the anisotropy parameter a, have to be determined for each mode from non-linear data. This large number of parameters seems to be a drawback. However, physical guidelines, related to the structure of the Pompom

molecule, can be taken into account. The free ends of the molecule correspond to the fastest relaxation times combined with no, or less, equivalent branches q. Going to the center of the molecule, relaxation time and equivalent branches will increase. Moreover, the stretch relaxation time is constrained in the interval $\lambda_{0b,1-1} < \lambda_{s,i} \leq \lambda_{0b,i}$. The anisotropy parameter a should decrease for increasing q. A low value for q represents the ends of the molecules, which relax by a highly anisotropic movement (primitive path fluctuations), while high q values reflect the inner parts of the molecules where constraint release becomes more important, making the relaxation more isotropic, i.e.. $a \rightarrow 0$.

The Pompom model can also be formulated in terms of two equations, which reflect more clearly the two relaxation mechanisms: one for the stretch and one for the orientation. Here, in the extended Pompom model, the stretch and orientation are combined into one equation that is less transparent. However, in case of $a = 0$ two situations can be distinguished:

- Only orientation relaxation for low strains ($\Lambda \approx 1$; part (a) and (b) of Eq. (6) and Eq. (7) are equal to zero.)
- Only stretch relaxation for high strains ($\Lambda >> 1$; part (c) of Eq. (7) is equal to zero.)

Instead of the viscoelastic stress we have chosen to formulate the FIC model in terms of the volume invariant recoverable elastic strain tensor $\mathbf{B}_e$, since we consider this to be a representative measure for the orientation and stretch of the molecules.

Quiescent crystallization

For quiescent crystallization, leading to spherulitical structures, the set of equations reads [2,11,12]

$$\begin{aligned}
\dot{\phi}_3 &= 8\pi\alpha \quad (\phi_3 = 8\pi N) \quad \textit{'rate'} \\
\dot{\phi}_2 &= G\phi_3 \quad (\phi_2 = 8\pi R_{tot}) \quad \textit{'radius'} \\
\dot{\phi}_1 &= G\phi_2 \quad (\phi_1 = S_{tot}) \quad \textit{'surface'} \\
\dot{\phi}_0 &= G\phi_1 \quad (\phi_0 = V_{tot}) \quad \textit{'volume'}
\end{aligned} \tag{12}$$

in which α is the nucleation rate and G is the crystal growth rate. Impingement and

swallowing are disregarded, i.e. nucleation does not depend on the volume of crystallized material. This set of equations fully characterizes the spherulitical structure, i.e. the mean specific number of spherulites N, their radius R_{tot}, surface S_{tot} and volume V_{tot}. The set is combined with the Avrami model for spherulitical impingement

$$\phi_0 = -\ln(1-\xi_0) \tag{13}$$

in which ξ_0 is the degree of space filling.

Flow-induced crystallization

For flow-induced crystallization, the set of differential equations reads [11,12]

$$\begin{aligned}
&\dot{\psi}_3 + \tfrac{1}{\tau_n}\psi_3 = 8\pi J_2 g_n \quad (\psi_3 = 8\pi N_f) \quad \textit{'rate'} \\
&\dot{\psi}_2 + \tfrac{1}{\tau_l}\psi_2 = \psi_3 J_2 \tfrac{g_l}{g_n} \quad (\psi_2 = 4\pi L_{tot}) \quad \textit{'length'} \\
&\dot{\psi}_1 = G\psi_2 \quad (\psi_1 = S_{tot}) \quad \textit{'surface'} \\
&\dot{\psi}_0 = G\psi_1 \quad (\psi_0 = V_{tot}) \quad \textit{'volume'}
\end{aligned} \tag{14}$$

in which J_2 the second invariant of the deviatoric part of the recoverable strain tensor[1] (that is why Zuidema [11] named the model $S(J_2)$-model).

$$J_2(\mathbf{B}_e^d) = \tfrac{1}{2}\mathbf{B}_e^d \cdot \mathbf{B}_e^d \tag{15}$$

As with quiescent crystallization, impingement and swallowing are disregarded and impingement also is modeled with an Avrami model. Since both, spherulitical and flow induced structures contribute to the degree of space filling, they are combined in one model for impingement

$$\phi_0 + \psi_0 = -\ln(1-\xi_0) \tag{16}$$

in which ξ_0 is the total degree of space filling. Notice that the set of Eqs (14) is solved for every mode of a multi mode viscoelastic model, i.e. every mode has its own

[1] It is interesting to see the equivalence of this tensor, and its second invariant, with the tensor order parameter as defined in the Onsager theory[8] for the transition from isotropic to nematic of non-dilute solutions of rod-like molecules. This order parameter is defined as the deviatoric part of the orientation configuration tensor $\mathbf{S} = .\langle \mathbf{uu} \rangle$. The maximum of the scalar order parameter S by: $S^2 = 3/2\ \mathbf{S}:\mathbf{S}$.

contribution to flow induced nucleation and crystallization. Assuming that the parameters in Eqs (14) are the same for all modes implies that the mode with highest relaxation time, representing the high molecular weight relaxation effects, will contribute the most. From the eigenvectors of the recoverable strain tensor $\mathbf{B_e}$ the corresponding, local orientation is determined. Again, notice that this reflects the orientation of the segments of the high molecular weight part of the molecular weight distribution. This set of equations gives a full description of the flow-induced oriented, crystalline structure; i.e. the specific number of flow-induced nuclei N_f and the total length $L_{f,tot}$, surface $S_{f,tot}$, and volume $V_{f,tot}$. The relaxation time τ_n for the nuclei, the relaxation time τ_l for the shish, and the scaling parameters g_n and g_l, have to be determined to complete the model. (In the case of the Eder model [2], the driving force for flow induced crystallization is the shear rate $\dot{\gamma}$ and J_2 should be replaced by $\dot{\gamma}^2$ and the values of the parameters g_n and g_l should be adapted.)

Both crystallization models can be combined with a model for impingement as for example the Avrami model

$$-\ln(1-\xi_g)=\phi_0+\psi_0 \tag{17}$$

in which ξ_g represents the degree of space filling. The overall degree of crystallinity ξ is obtained by multiplying the degree of space filling ξ_g with the degree of crystallinity in each spherulite/shish-kebab.

As nucleation sites are considered to act as physical cross links, the maximum rheological relaxation time θ_j is coupled with the number of nucleation sites. This reflects the idea that within the flow-induced nucleation event, preferentially the high molecular weight tail molecules are involved. The simplest linear relationship is chosen

$$\theta_j=a_T(T)\theta_{j0}\left(1+\frac{\varepsilon N_f}{g_n}\right) \tag{18}$$

The interplay between rheology and flow induced crystallization can, therefore, be rather complex. The model is implemented in VIp, a FEM-code for the numerical simulation of the injection molding process [13].

Results

In the following, quantitative results for shear flow are summarized that were discussed in more detail in Zuidema [11] and Zuidema et al. [12]. Next, qualitative results for planar elongation flow from Swartjes [7] are presented. Results being quantitative or qualitative depend on the available set of input data. For the polymer used in the shear flow, all input parameters -except extensional data- were available. Since the Leonov model is applied here, this is not an objection and computations can be quantitative. For the polymers used in the extensional flow, the Pompom model was applied as well and thus extensional data are required. However, for the polymer for which their data were available, the parameters for the FIC model were not obtained yet.

Shear

Due to their larger relaxation times, high molecular weight molecules will facilitate nucleation/ crystallization and, therefore, it is postulated that the flow-induced structures will correlate most strongly with the viscoelastic mode with the highest relaxation time. Or, more formal, the number of flow-induced nuclei and/or the growth rate of the flow-induced structures are a functional of the invariants of the elastic Finger tensor corresponding to the highest relaxation time. If this statement is true, then material that experienced a history leading to the same value of this (unknown) functional should show the same flow-induced structure and, thus, the same optical properties.

Computational results were compared with short-term shear experiments (duct flow) for different wall shear rates and different shear times performed by Jerschow [5]. The polymer was an iPP (K2Xmod, Borealis). The distance from the wall of the boundaries of flow-induced oriented and fine-grained layers were determined optically. These clearly visible transitions were used to verify the idea postulated in the beginning of this section. The comparison was done by correlating the shear time with the number of flow induced shish in the case that the relaxation time for shish generation is taken infinity. For both flow rates applied (79 and 115 [s^{-1}]) and each shear time the value of this integral was calculated at the experimentally determined transition positions. The parameters in the model are obtained by fitting only one benchmark experiment (wall shear rates 72 [s^{-1}], shear time 7 [s]).Details on the determination of the parameters in the FIC model can be found in [5] and [11]

It is clearly seen that the values for this time integral are almost constant for the

mode with the largest relaxation time (Figure 2 left) while they vary strongly, albeit linear with shear time for the other modes (only one shown). This supports the basic concept stated above that the flow-induced structures correlate most strongly with the viscoelastic mode with the highest relaxation time and, therefore, this is a good candidate for the driving force in a model for flow-induced crystallization.

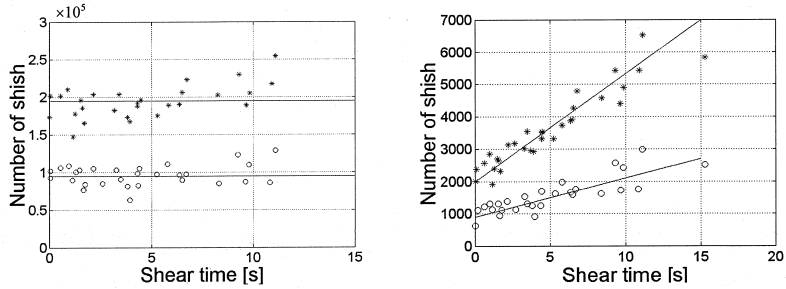

Figure 2. Calculated number of Shish at the experimental measured positions of the layer transitions as a function of the shear time. Oriented/fine grained (top line), grained/normal (bottom line) for experiments with wall shear rates of 79 [s^{-1}] and 115 [s^{-1}]. Results are given for mode 1 (left) and mode 2 (right).

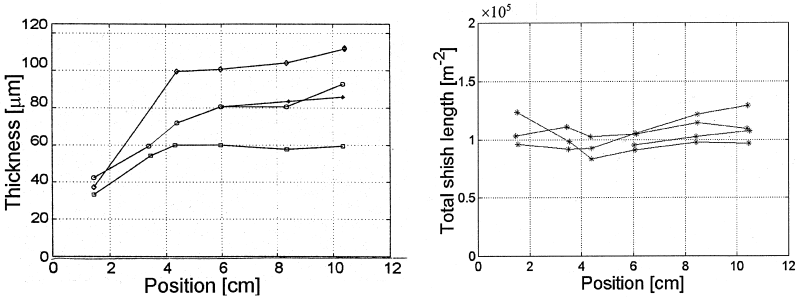

Figure 3. Left: measured boundary layer thickness as a function of the position in the duct for different flow rates, (11.3, 9.9, 7.9, 5.7).10^{-7}[m^3s^{-1}]. Right: calculated values for the specific total shish length at the measured positions.

For further model validation, simulations were carried out for steady state flow for the same material and compared with experimental results (see Eder [2]) in the same way as before. Numerically, quenching was imposed by forcing the wall temperature to be T_w = 293 [K]. Results are shown in Figure 3. In Figure 3 (left) the measured thickness of the oriented layer as a function of the position in the duct is given for a range of flow rates. Figure 3 (right) gives the specific total shish length at these positions. It is seen that, within experimental error, a constant value is obtained at the layer boundaries, which supports the presented model.

Elongation

Swartjes [7] developed a cross-slot flow cell to investigate the crystallization behavior in a complex flow with a strong extensional component. As the focus in Swartjes work was on the development of experimental methods, the behavior of the constitutive models in this type of flows was studied in a qualitative way.

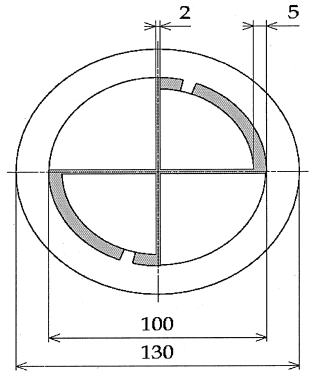

Figure 4. Dimensions in [mm) of the cross-slot flow cell.

The experimental work contained both, birefringence measurement as well as Wide Angle X-ray Scattering (WAXS) to study real time structure development. From both methods it was found that the flow could cause a highly oriented structure developed around the outflow centerline.

Calculations were done for two iPP's (DSM13E10, Borealis Daplen KS10). However, the parameter sets for both materials were incomplete. DSM13E10 was characterized rheologically, both in shear and elongation, but the parameters for flow induced crystallization (FIC) model are unknown yet. This material is, therefore, used to compare the stresses predicted by the two viscoelastic models. The extensional behavior of Daplen KS10 could not be characterized, but the FIC parameters are available. Therefore, this material is used to show the behavior of the FIC model in the cross-slot flow, in more detail while using the Leonov model only.

The schematic of the cross-slot flow cell together with its dimensions, are given in Figure 4. It consists of two curved reservoirs and a cross-slot. Flow is created by rotating two cams which are connected to the outer ring over 90 degrees. A stagnation line will occur in the center of the cross-slot. Depth of the channels and reservoirs is 2

[mm]. The maximum obtainable strain rate in the center is about 10 [s^{-1}]. The total maximum strain of particles traveling close to the stagnation line is about 10 [-]. Using three thermal baths controls the temperature history.

In his experiments with the cross-slot flow cell, Swartjes [7] made some typical observations with both, birefringence and WAXS, for the DSM13E10 iPP. Applying flow at a temperature around 418 [K], a temperature at which noticeable quiescent crystallization effects take hours, led to a narrow band of a fiber-like crystalline structure around the outflow centerline which did not relax anymore (see Figure 5 top).

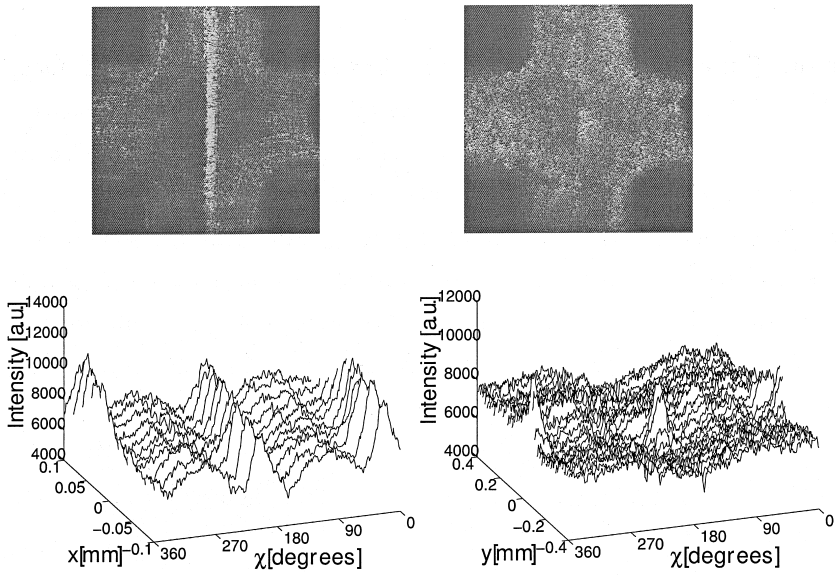

Figure 5. Field-wise birefringence (top) and WAXS measurements (bottom) for DSM13E10: Top left: 10 minutes after flow stoppage, right: after 30 minutes (the bright central structure is less clear visible as overall crystallization sets in), bottom left: WAXS intensity for the (110) reflection vs. orientation angle and position on the inflow centerline, bottom right: same on the outflow center line.

At 428 [K], no distinguishable like-like structures were seen before all-over crystallization occurred. From WAXS measurements, using the micro-focus-beam-line ID13 (beam size 30 [μm]) at the European Synchrotron Radiation Facility (ESRF), it was found that the width of this narrow band was in the order of 80 [μm], see Figure 5 bottom, where the integrated WAXS intensity is given for the (110) refection as a

function of the position perpendicular and parallel to the outflow direction.

Numerical simulations were performed to check whether these observations could be predicted in a qualitative way by the previously described FIC-model. Figure 6 shows the computed flow-induced space filling in the center plane of the cross-slot flow cell using the parameter set of the Daphlen KS10 iPP. For symmetry reasons, only a quarter of the central area of the flow cell is shown. A very sharp, highly crystalline, narrow band is also found in the simulations. Taking a level of 20% space filling as a threshold, the band has a width in the order of 100 [μm].

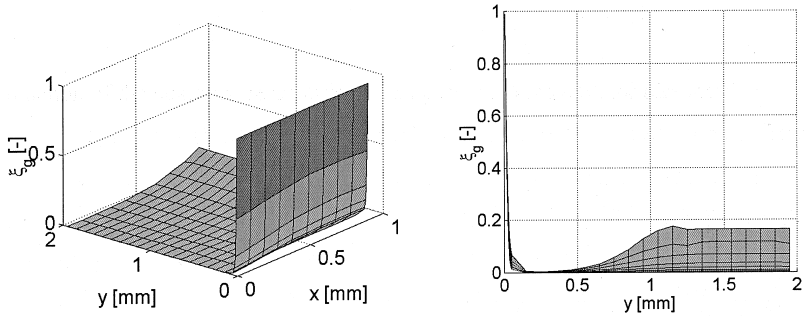

Figure 6. Prediction of the space filling in the cross-slot flow cell in the midplane for Daplen KS10 after applying a flow rate of 1.85 10-8 [m^3s^{-1}] for 40[s], and waiting 800[s] at 413 [K]. Left: 3D view, right: side view.

For this kind of flow it is important to have a viscoelastic model that is predictive for the extensional stresses, i.e. the Pompom model instead of the Leonov model. The influence of the viscoelastic model is demonstrated in Figure 7 where the first normal stress difference in the midplane is shown (the predicted shear stresses are about the same, as expected, and not shown here). Around the outflow centerline the Leonov model predicts about twice higher normal stress levels than the Pompom model . This is due to the different behavior of the two models in extensional flow for which it is known that the Leonov model does a poor job. Of course this is reflected in the FIC behavior too, but this isn't further analyzed since the FIC parameters are not available for this material.

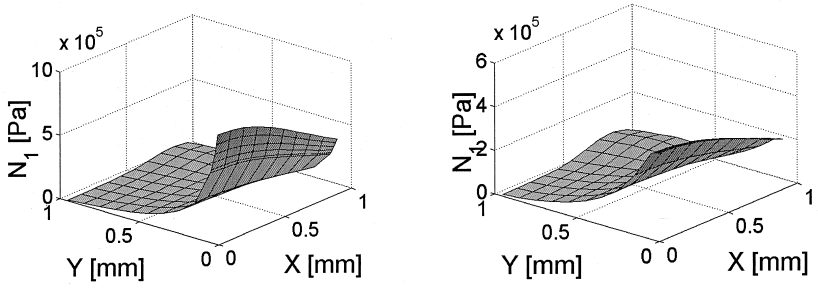

Figure 7. Predicted first normal stress difference. Left: Leonov, right: Pompom.

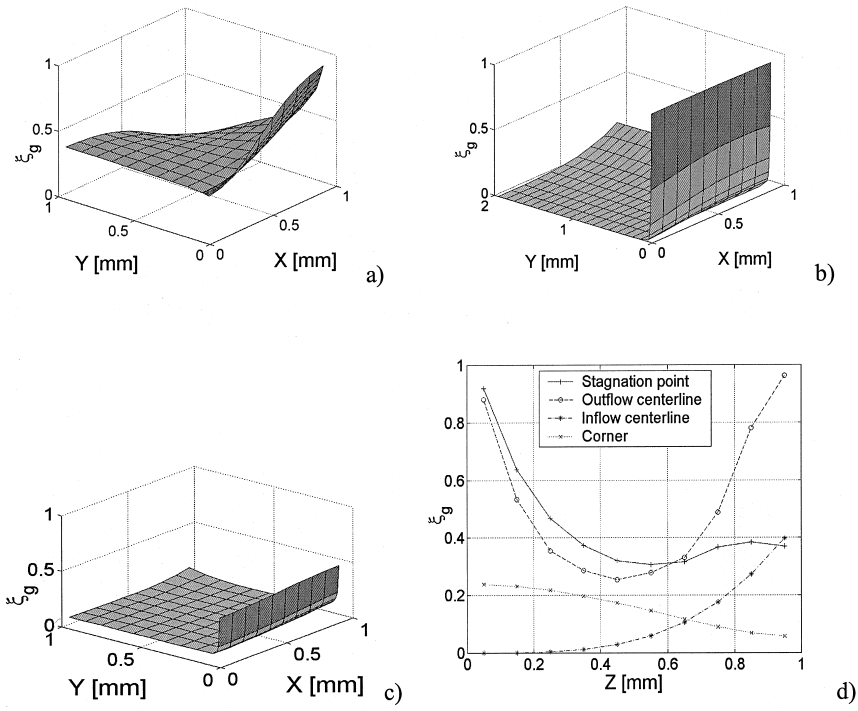

Figure 8. Predicted flow induced space filling. a) plane at z=0.95[mm], b) plane at z=0.05 [mm], c) mean space filling, d) space filling distribution over the flow cell depth in four specific points. Coordinates (x,y) in [mm]: Stagnation point: (10^{-6}, 5.10^{-3}), outflow centerline: (0.9, 5.10^{-3}), inflow centerline: (10^{-6}, 0.95), point near the corner: (0.9, 0.95).

Finally, we want to stress the importance of a computational model when performing a complex experiment, as is the cross-slot flow. Due to three-dimensionality of this flow, also a three-dimensional distribution of the crystalline structures and crystallinity is generated. Only a computational model can show these effects and help to understand the influence on the birefringence [14,15] and WAXS experiments.

Figure 8 (a,b) shows the flow induced space filling in two planes in the cross slot cell and the mean space filling (c). In Figure 8 (d) the distribution over the depth of the flow cell at some specific points is shown. Both figures demonstrate how strongly the distribution can vary. In Swartje [7] it is demonstrated how this distribution can be made more two-dimensional by adapting the flow conditions. This design of an experiment is only possible with the aid of the numerical model.

Discussion

A model is presented that allows for the prediction of the crystalline structure distribution in products that experienced a complex thermo-mechanical history. The driving force for flow-induced nucleation and crystallization is the molecular orientation, in particular the orientation of segments of the high-end tail molecules. This is accounted for by taking only the order parameter obtained from the viscoelastic mode with the highest relaxation time. Moreover, there is direct feedback of the nucleation process, since the generated nuclei are considered to act as physical cross links, which increase the highest relaxation time. These couplings are kept as simple as possible via a linear relation. More work is needed to establish the true nature of these relations. The model is validated by comparing numerical with experimental results for shear flow from the literature and the agreement is good. For extensional flow only qualitative agreement was obtained due to a lack of input data.

In the near future, the predicted crystalline structure will be used as the input for the determination of the final product properties. For example, with the detailed description of the crystalline structure and knowing the PVT behavior [16], the density distribution and residual stresses in a product can be computed. Next, the prediction of dimensional stability for semi-crystalline polymers becomes a realistic option (as comparable to amorphous polymers, see for example Caspers [13]).

[1] W. Schneider, A. Köppl, and J. Berger, *Int. Polymer Processing* **1988**, *3*, 51
[2] G. Eder, H. Janesschitz-Kriegl, and S. Liedauer, *Prog. Polym. Sci.* **1990**, *15*, 629
[3] B. Schrauwen, L. Govaert, G.W.M. Peters, H.E.H. Meijer, *Macromol. Symp* **2002**, this special issue
[4] S. Vleeshouwers and H.E.H. Meijer, Rheologica Acta **1996**, *35*, 391
[5] P.Jerschow, PhD Thesis, Johannes Kepler University, Linz, Austria, **1994**
[6] W.M.H. Verbeeten, G.W.M. Peters, F.P.T. Baaijens, J. Rheolog, **2001**, *4*, 823
[7] F. H. M. Swartjes, PhD Thesis (available on: www.mate.tue.nl), Eindhoven University of Technology, The Netherlands, **2001**
[8] R.G. Larson, *The Structure and Rheology of complex fluids*, Oxf. Univ. Press, 1999
[9] T.C.B. McLeish and R.G.B. Larson, *J. Rheolog*, **1998**, *42*, 81
[10] R.B. Bird, C.F. Curtiss, R.C. Armstrong, O. Hassager, *Dynamics of Polymeric Liquids, Vol II, Kinetic Theory*, John Wiley and Sons, 1987
[11] H. Zuidema, PhD Thesis (available on: www.mate.tue.nl), Eindhoven University of Technology, The Netherlands, **2000**
[12] H. Zuidema, G.W.M. Peters, and H.E.H. Meijer, *Macromol. Theory and Simulation*, **2001**, *4*, 447
[13] L. W. Caspers, PhD Thesis (available on: www.mate.tue.nl), Eindhoven University of Technology, The Netherlands, **1995**
[14] J.F.M. Schoonen, PhD Thesis (available on: www.mate.tue.nl), Eindhoven University of Technology, The Netherlands, **1998**
[15] A.C.B. Bogaerds, W.M.H. Verbeeten, G.W.M. Peters, F.P.T. Baaijens, *Comp. Meth. in Appl. Mech. Eng.* **1999**, *180*, 41
[16] H. Zuidema, G.W.M. Peters, H.E.H. Meijer, *J. Appl. Pol. Sci.* **2001**, *82*, 1170